UNIVERSITY OF COPENHAGEN

A thesis presented to the Faculty of Physics in partial fulfillment
of the requirements for the degree

Master of Physics

Developing a Method for High Resolution Water Isotope Measurements in Ice Cores

Kerttu Maria Peensoo

Supervisors: Vasileios Gkinis, Yang Zhang, Thomas Blunier

May 2021

Acknowledgements

First and foremost I would like to thank my main supervisor Vasileios Gkinis and mechanical engineering intern Simon Fassel who worked on this project with me. I am also grateful for Karl-Emil Nielsen who helped me with electronics and mechanical engineering. Next I want to thank Yang Zhang who helped to organize experiments at DTU.

I also want to thank Iben Koldtoft, who helped me with all the countless orders. Next I want to thank Steffen Bo Hansen and Thomas Blunier with helping to set up the designated laser ablation lab. Also thanks to Thea, Mikkel and all the others at PICE.

I finally want to thank Kaur for always believing in me and supporting me throughout my thesis.

Abstract

In this thesis a laser ablation system is developed for the purpose of water isotope measurements in ice. Laser ablation allows for extraction of water vapour from ice, which can then be analyzed with cavity ring down spectrometry. This work explains the advantages of this system compared to continuous flow analysis and discrete sampling. A full scale system is built and tested at the department of the Physics of Ice, Climate and Earth.

Keywords: cavity ring-down spectrometry; hydrogen-2; isotope measurements, methods and equipment; ice core studies; laser ablation; oxygen-18

Motivation

The glacial ice on the poles can be thought of as a climate archive of Earth. On the polar ice sheets, snow accumulates faster than it ablates. Over time, snow from each year of snowfall is added to the surface of the ice sheet. The snow eventually gets compressed into ice under the weight of the new snow. Not all ice is identical, its composition is dependent on the climate conditions under which it formed. One way in which these differences occur is in the variation of the water isotopes that make up the ice. Measuring the differences in isotopic ratios enables us to distinguish between summers and winters. This creates a distinctive layered pattern, similar to annual rings in trees. This makes it possible to count the annual layers corresponding to individual years, providing a method relate the age of an ice core to the depth from where it was drilled. The ratios of water isotopes also contain information about past temperatures.

The Beyond EPICA project aims to obtain the oldest accessible ice core (1.5 million years old), from deep within the antarctic ice sheet. The ice is scheduled to be available for analysis in 2024. For very deep ice core, the annual layers are extremely thin, with 10000 years of ice compressed into a single meter of ice. Investigating such an ice core requires the development and adoption of new experimental techniques that offer a precise and non-destructive way of analyzing the ice samples. One such method is laser ablation, which uses a powerful short-pulsed laser to ablate microscopic holes into an ice sample, without melting or damaging the bulk of the material. Laser ablation is widely used for machining metals, but has not found widespread adoption in ice core research. This thesis aims to make use of this valuable method, by developing a laser ablation system compatible with the requirements of water isotope measurements of ice.

Contents

List of Figures

CHAPTER 1

Introduction

1.1 Water Isotopes in Ice Cores

Isotopes in Water

Chemical elements are defined by the number of protons in their nuclei. Atoms, whose nuclei differ only in the number of neutrons are called isotopes. Isotopes can be divided into two categories: radioactive and stable isotopes. Radioactive isotopes emit radiation while they decay into other chemical elements. The duration of the decay is described by the half-life, which is the time it takes for half of the mass to decay. Stable isotopes don't decay over time or their half-life is so long that they haven't been observed to.

Water consists of naturally abundant stable isotopes of hydrogen and oxygen. These are called water isotopes and their masses and relative abundances are shown in Table 1.1. The most common isotopes are ^{1}H and ^{16}O which both have an occurrence frequency greater than 99%. The other stable isotopes are deuterium (D) for hydrogen and ^{17}O and ^{18}O for oxygen which all occur less than 1% of the time. Deuterium has one more neutron than hydrogen. ^{17}O and ^{18}O have one and two more neutrons than ^{16}O, respectively. The additional neutrons give these isotopes a higher mass than their more commonly found counterparts.

Isotope	Mass in u	Abundance in %
^{1}H	1.0078250321(4)	99.9850(70)
D (^{2}H)	2.0141017780(4)	0.0115(70)
^{16}O	15.9949146221(15)	99.757(16)
^{17}O	16.99913150(22)	0.038(1)
^{18}O	17.9991604(9)	0.205(14)

Table 1.1: Natural abundances and masses of stable hydrogen and oxygen isotopes.[1]

Delta Notation and Water Isotopes in the Global Water Cycle

The isotopic abundance of water can be characterized as a deviation from the standard using the delta notation

$$\delta^{i} = \left(\frac{{}^{i}\mathrm{R}_{\mathrm{sample}}}{{}^{i}\mathrm{R}_{\mathrm{standard}}} - 1 \right) \cdot 1000, \tag{1.1}$$

where ^{i}R is the isotopic ratio and the multiplication by thousand gives units in ‰. The standard used internationally for water isotopes is VSMOW (Vienna Standard Mean Ocean Water). Therefore for the two most studied water isotopes we have the following.[2]

$$\delta D = \left(\frac{\left(\frac{\mathrm{D}}{\mathrm{H}}\right)_{\mathrm{sample}}}{\left(\frac{\mathrm{D}}{\mathrm{H}}\right)_{\mathrm{VSMOW}}} - 1 \right) \cdot 1000 \qquad \delta^{18}O = \left(\frac{\left(\frac{^{18}\mathrm{O}}{^{16}\mathrm{O}}\right)_{\mathrm{sample}}}{\left(\frac{^{18}\mathrm{O}}{^{16}\mathrm{O}}\right)_{\mathrm{VSMOW}}} - 1 \right) \cdot 1000 \tag{1.2}$$

The value of δ changes throughout the global water cycle. Figure 1.1 shows the approximate change in δ, taking that for the subtropical ocean ${}^{i}\mathrm{R}_{\mathrm{sample}} = {}^{i}\mathrm{R}_{\mathrm{standard}}$ and therefore $\delta = 0$‰. The heavy water molecules (e.g. $\mathrm{D_2}^{16}\mathrm{O}$, $^{1}\mathrm{H_2}^{18}\mathrm{O}$) have lower water vapour pressure than the light water molecules ($\mathrm{H_2}^{16}\mathrm{O}$). Consequently, the heavier water molecules have a lower tendency to evaporate and a higher tendency to condensate. This gives arise to the phenomenon called fractionation meaning that a condensate and its associated vapour have different isotopic composition.[3]

When the water evaporates from the subtropical ocean, it gets depleted from heavy isotopes as lighter isotopes evaporate more easily. Then, as the water vapour is being carried from mid-latitudes towards high-latitudes, the δ value decreases further because heavier water isotopes have a higher tendency to condense to form precipitation. As a result, the δ value of precipitation is offset from the δ value of the water vapour. Finally, the snow that accumulates on the ice sheet has considerably less heavy water isotopes compared to the subtropical ocean.[3]

Annual Layers in Ice Cores

The amount of snowfall in polar regions differs from summer to winter. In the summer months, it snows considerably more than in winter. Therefore, the δ value in summer is larger than in winter because

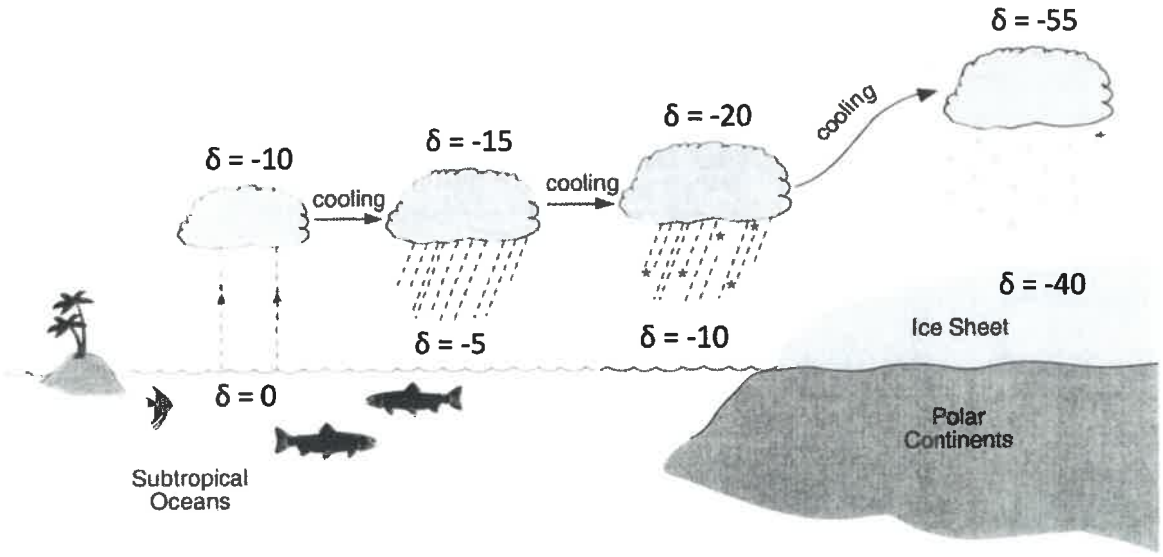

Figure 1.1: Conceptual model of isotopic change in the water cycle. Adapted from [4].

the heavy isotopes accumulate with the snowfall. From year to year this effect produces annual layers of variable δ values. In polar regions, the accumulation rate of snow is higher than the ablation rate of snow. Thus, water isotope data is being stored as the accumulating snow gets compressed into firn and then ice.

The annual layers play an important role in the dating of ice cores. Analyzing water isotopes enables us to identify and count the annual layers in the ice. Combining this information with the measured depth from which the ice sample was extracted allows us to link the depth of the core to the age of the core. Knowing the age of the ice core allows us to relate the physical and chemical properties of that ice to the climate conditions that existed at the time of its formation.

Firn is the stage between snow and ice, and it forms as snow keeps accumulating on the surface of glacier ice. The thickness of annual layers in the firn zone is influenced by the weight of the overlaying firn. The transition from firn to glacier ice takes place once the density has reached the density of ice ($917 kg/m^3$) and cannot be compressed any further.

The deeper a given annual layer is, the thinner it is, since it is thinned over time by ice flow, which is a highly viscous flow of the ice occurring over the timescale of thousands of years. The rate of ice flow depends on where the ice core site is located with respect to the ice divide. An ice divide is the boundary of two ice sheets from which two opposite downstream flow directions of ice begin. When moving away

from the ice divide, the annual layers become progressively thinner due to the strain caused by the ice flow. Figure 1.2 features the decrease in observed annual layer thickness with the increasing ice core depth of the GISP2 central Greenland core.

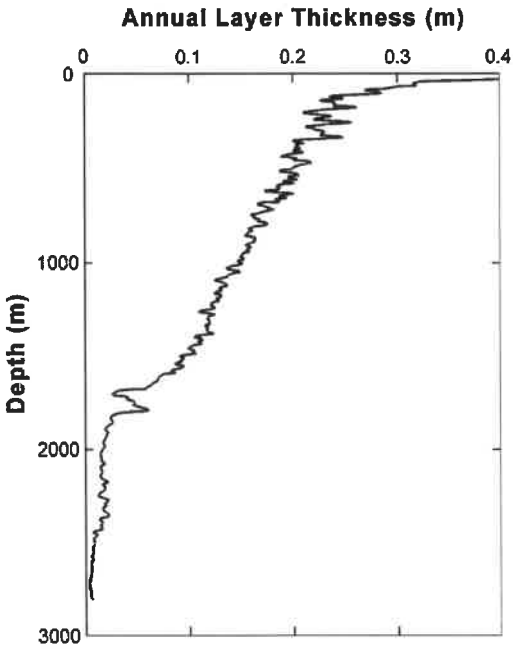

Figure 1.2: Decrease in observed annual layer thickness versus the depth of the GISP2 central Greenland core. Taken from [3]

Connection to Past Temperatures

The connection between water isotopes and past temperatures can be obtained by combining results from climate models and real water isotope measurements from ice cores. In this section we present two ways to relate water isotopes to temperature.

The climate proxy for temperature is $\delta^{18}\mathrm{O}$, as the mean annual surface temperature T can be linked to the $\delta^{18}\mathrm{O}$ of snow by the following linear equation

$$\delta^{18}\mathrm{O} = \alpha \cdot T - \beta, \tag{1.3}$$

where α and β are constants. Analyzing the water isotope data from drilling stations at West and South Greenland the best values for the constants have been found to be $\alpha = 0.67 \pm 0.02$ and $\beta = (13.7 \pm 0.5)‰$.[5]

Equation 1.3 might not account for the temporal changes in ice cores, in which case another non-linear

relationship between the $\delta^{18}O$ and surface temperature T is used.

$$T = \alpha + \beta \cdot \delta^{18}O + \gamma \cdot (\delta^{18}O)^2 \tag{1.4}$$

Here α, β and γ are constants acquired by modelling the borehole temperature profile and fitting it to the measured temperature profile using the least-squares method.[6]

In addition, the deviation from the Global Meteoric Water Line (GMWL) can be used as a proxy for temperature. The GMWL is a linear relationship defined as

$$\delta D = 8 \cdot \delta^{18}O + 10‰ \tag{1.5}$$

and the measurements of precipitation worldwide have shown that $\delta^{18}O$ and δD can be fitted with Equation 1.5. Deuterium excess d is used to describe the deviation from the meteoric water line and is defined as

$$d = \delta D - 8 \cdot \delta^{18}O \tag{1.6}$$

Precipitation over the ocean at tropical and subtropical regions has a deuterium excess value of $d \approx 10‰$. The value of d in polar ice sheets is influenced by the change of relative humidity and sea-surface temperature at the source region.[3]

Considering only small-magnitude isotopic changes, we can write

$$\Delta\delta D = \gamma_{\text{site}} \cdot \Delta T_{\text{site}} - \gamma_{\text{source}} \cdot \Delta T_{\text{source}} + \gamma_{\text{m}} \cdot \Delta\delta^{18}O_{\text{m}}, \tag{1.7}$$

$$\Delta d = -\beta_{\text{site}} \cdot \Delta T_{\text{site}} + \beta_{\text{source}} \cdot \Delta T_{\text{source}} - \beta_{\text{m}} \cdot \Delta\delta^{18}O_{\text{m}}, \tag{1.8}$$

where T_{site} and T_{source} are the ice-core site and the vapour source region temperatures respectively, $\Delta\delta^{18}O_{\text{m}}$ is the ocean isotopic composition, γ and β are positive coefficients that have been estimated from isotopic models for central East Antarctica. Temperature histories for the ice sheet and the source region can be obtained by solving the two relations together using measurements of $\delta^{18}O$ and δD from an ice core. This gives

$$\Delta T_{\text{source}} = \gamma_{\text{site}} \cdot \Omega \cdot \Delta d + \beta_{\text{site}} \cdot \Omega \cdot \Delta\delta D + \gamma_{\text{site}} \cdot \beta_{\text{m}} - \beta_{\text{site}} \cdot \gamma_{\text{m}} \cdot \Omega \cdot \Delta\delta^{18}O_{\text{m}}, \tag{1.9}$$

$$\Delta T_{\text{site}} = \gamma_{\text{source}} \cdot \Omega \cdot \Delta d + \beta_{\text{source}} \cdot \Omega \cdot \Delta\delta D + \gamma_{\text{source}} \cdot \beta_{\text{m}} - \beta_{\text{source}} \cdot \gamma_{\text{m}} \cdot \Omega \cdot \Delta\delta^{18}O_{\text{m}}, \tag{1.10}$$

where $\Omega = \gamma_{\text{site}} \cdot \beta_{\text{source}} - \gamma_{\text{source}} \cdot \beta_{\text{site}}$. Using the measured δD and d data, the ΔT_{source} and ΔT_{site} can be determined as deviations from present day values.[7]

1.2 Detecting Water Isotopes

There are two methods that have commonly been used to detect water isotopes in ice cores. Both of those methods have their own special requirements on how to prepare the ice sample prior to the measurement.

This chapter gives an overview of the working principles of Isotope Ratio Mass Spectrometry and Cavity Ring-Down Spectroscopy as well as techniques for preparing the ice core sample for measurement.

Isotope Ratio Mass Spectrometry

Isotopes of different chemical elements can be detected using an Isotope Ratio Mass Spectrometer (IRMS), which uses the mass difference of isotopes to determine isotope ratios in a sample. The principal components of an IRMS are the source, the analyzer and the detector assembly.[8]

The sample is first introduced into the source by injecting it into the IRMS through an inlet. Then the sample is vaporized by a heater and ionized by bombarding the sample with accelerated electrons. The ionized sample is then focused into a coherent beam and accelerated down the flight tube to the analyzer. The analyzer is the region where different isotopes in the sample are separated. This happens when the incoming beam of the ionized sample goes through a magnetic field in the flight tube. The ionized sample moving through the flight tube experiences Lorentz force F_{L} inside the magnetic field and gets deflected based on its mass to charge ratio as the magnetic force supplies the centrifugal force F_{C} acting on the ions. Assuming that the magnetic field is perpendicular to the trajectory of an ion, we get

$$F_{\mathrm{L}} = F_C \quad \rightarrow \quad q \cdot v \cdot B = \frac{m \cdot v^2}{r} \quad \rightarrow \quad q \cdot B = \frac{m \cdot v}{r} \tag{1.11}$$

where q, m, v are the charge, mass and speed of the ion respectively, B the magnetic field, and r the curvature radius of the ion's trajectory. The trajectory of an ion is described by the radius of its curvature

$$r = \frac{m}{q} \cdot \frac{v}{B}, \tag{1.12}$$

and is proportional to the mass to charge ratio. The detector assembly consists of multiple detectors, which are positioned at the expected arrival points of each of the relevant isotopes within the sample. Sampling the distribution of the ions with the detectors allows us to infer the isotopic ratio of the sample.[8]

The preparation of a sample for measurements of isotopic ratio with an IRMS is different for ^{18}O and deuterium. In order to prepare for measuring the former, the ice sample is melted and frozen repeatedly, while pumping the chamber to remove any non-condensible gases, that may have been trapped in the ice. Then the ice is melted again and CO_2 is introduced into the sample. The amount of CO_2 is approximately 1/200 of the sample in moles. This starts the equilibration process, which is done in a bath thermostated at 25.3°C over the course of three days. During the equilibration process the flask with the sample is frequently shaken in order to ensure that ^{18}O is not condensed onto the walls of the flask. The water level in the bath is kept just above the closed flask to prevent cooling and minimize the condensation.

After the equilibration, the process

$$C^{16}O^{16}O + H_2{}^{18}O \iff C^{16}O^{18}O + H_2{}^{16}O \tag{1.13}$$

is in balance and the CO_2 will have obtained the same isotopic ratio as the sample. Then an aliquot of 3cc of CO_2 is drawn from the flask using a gas pipette system and directed into the IRMS for isotopic ratio measurements. Another 2 to 3 aliquots of CO_2 are taken from the same sample-CO_2 mixture and measured with IRMS to make sure that the equilibration has been attained.[9]

In order to measure the isotopic ratio of deuterium, the standards and melted ice samples are prepared in small vials, which are put into an autosampler. Each vial contains about 1ml of water from which an aliquot of 50µl is drawn by the autosampler for analysis. Most of the aliquot is used to flush the valve connected to the inlet system that interfaces with the IRMS, 5µl of the sample is injected to the glass inlet system, where it is slowly directed to a uranium furnace maintained at 600°C. The first part of the inlet system is then closed off and the reaction between the sample and the uranium

$$H_2O + U \implies H_2 + UO \tag{1.14}$$

produces uranium oxide which remains in the furnace and the hydrogen gas containing the isotopic data of interest is directed into the IRMS. After the measurement, the inlet system is evacuated with a vacuum pump in order to reduce the amount of water left from the previous sample in order to avoid memory effects between samples.[10]

Cavity Ring-Down Spectroscopy

Another way of detecting water isotopes is using an infrared cavity ring-down spectrometer (CRDS) which makes use of photoabsorption by water molecules. The key components of a CRDS are an infrared laser, a high finesse optical cavity which consists of two or more mirrors, and a photo-detector. The ice sample is prepared in the gas phase and injected into the optical cavity, and the ring-down measurement is performed, which consists of the following steps:

1. Light from the infrared laser enters the optical cavity through one partially reflecting mirror.
2. The light inside the cavity builds up over time and is monitored through a second partially reflecting mirror using a photo-detector.
3. Once the light intensity attains the maximum value, the laser is turned off rapidly and the exponentially decaying intensity is measured with the photo-detector. This is called a ring-down measurement.

When the laser is shut off, the remaining light confined within the cavity completes thousands of roundtrips during which it interacts with the sample until decaying completely. The time constant of this decay is referred to as the ring-down time

$$\tau(\nu) = \frac{l_c}{c[(1-R) + \alpha(\nu) l_c]}, \tag{1.15}$$

where ν is the wavelength of the light, l_c the length of the cavity, c the speed of light in vacuum, R the reflectivity of the mirrors and $\alpha(\nu)$ the absorption coefficient of the selected absorption feature. The absorption spectrum of the sample is obtained by measurement of τ at different laser wavelengths corresponding to the absorption features specific for the most common water isotopologues ($^1H_2{}^{16}O$, $^1H^2H^{16}O$, $^1H_2{}^{18}O$). $\delta^{18}O$ and δD are retrieved by comparing the measured absorption spectra to the spectrum of standard VSMOW.[11][12][13]

CRDS allows for simultaneous measurement of $\delta^{18}O$ and δD and there are no water isotope specific preparation methods required. However, since the CRDS still requires the sample to be in the gas phase, a controlled method of extracting water vapor from the ice is needed. At the Physics of Ice, Climate and Earth (PICE) section of Niels Bohr Insitute in the isotope lab, a commercially available CRDS such as the Picarro L2130-i is used for detecting water isotopes and the two methods used for sample preparation are Discrete Sampling and Continuous Flow Analysis (CFA).

Discrete Sampling

This section explains how preparation of the ice sample for discrete measurements with CRDS is performed at PICE. The ice with nominal length of 55cm is usually cut into either 11 or 22 pieces. Each piece is then put into a separate container marked according to the depth this part of the sample is acquired from, where they are then left to melt. Once all of the pieces from the ice sample are melted, a small aliquot of each are transferred into separate vials. The vials are then arranged into a tray in order of the depth that was noted on the container. One tray has space for 95 sample vials, fitting vials from around 4 or 8 ice samples with length of 55cm depending on amount of pieces they are cut in. Three additional vials consisting of different standards with known isotopic composition are put before the first sample in the tray. The standards are measured in the beginning and end of measuring all the samples in the tray in order to calibrate for instrument drifts. Once all the vials are in the tray, the tray is put into an autosampler, which is a commercially available complementing module to the CRDS.

The autosampler takes water from a vial with a syringe and injects it into an oven, where immediate evaporation of the entire sample is necessary to avoid fractionation effects producing an incorrect $\delta^{18}O$ and δD signal. The water vapour from the oven is directed into the CRDS for isotopic measurements. Multiple injections from the same vial are done and the results are averaged in order to increase

resolution and decrease memory effects. In addition, a carrier gas, either dry air or nitrogen, has to be connected to the CRDS during the measurements. The purpose of the carrier gas is to bring down the background water vapour level in the cavity of CRDS to below 500ppm. When a sample is injected to the cavity, the water vapour level rises to around 20000ppm, giving a clear distinction between background and signal.

The shortcomings of the preparation method for discrete measurement are the time and man-hours needed, as well as the limited spatial resolution of the ice stemming from the volume needed to perform the measurements. The time required to measure one tray of samples is 10 hours. Prior to measurement, the ice sample with nominal length of 55cm needs to be cut precisely into pieces. Melting the pieces and transferring them to vials as well as labeling them correctly involves a considerable amount of manual work. An ice sample that has been cut into 2.5cm or 5cm will correspond to a different amount of annual layers, depending on the depth of the origin of the ice core. This means that the CRDS measurement will have lower temporal resolution for deeper cores, since the measurement will represent the average of more years of isotopic data.

Continuous Flow Analysis

The Continuous Flow Analysis (CFA) system at PICE, shown in Figure 1.3, allows for simultaneous measurement of water isotopes, chemical impurities (e.g. Na^+, Ca^{2+}) and gases trapped in ice cores (e.g. CO_2, CH_4). The ice sample measured with the CFA system is an ice rod with dimensions $3.2 \times 3.2 \times 110$cm. The ice rod is extracted from the center of a cylindrical ice core to avoid parts that have been in contact with the drill and may include contaminants from handling. This is especially important for chemistry measurements.[14]

To run a measurement with CFA, the ice rod is first put into a freezer and continuously melted on a copper, cold-nickel coated melter at 20°C. The stable melting process is ensured by the stainless steel weight lying on top of the ice sample. An optical encoder connected to the weight records the vertical displacement of the steel weight, which is used to construct a depth scale for the measured data. The melter is built such that the meltwater from the outer part of the ice sample goes to waste to avoid contamination from the lab environment. The meltwater from the inner part of the ice rod is transported with the pump P1 to the debubbler. In the debubbler, gases are extracted from the meltwater of the sample, which is then directed to the valve V1.[14]

V1 switches between milliQ water and the sample. When one CFA run has been completed, meaning that one 110cm sample is melted, the system is flushed with milliQ water to have clear distinction between different CFA runs in the data. After V1, the lines to water isotope and chemical impurity

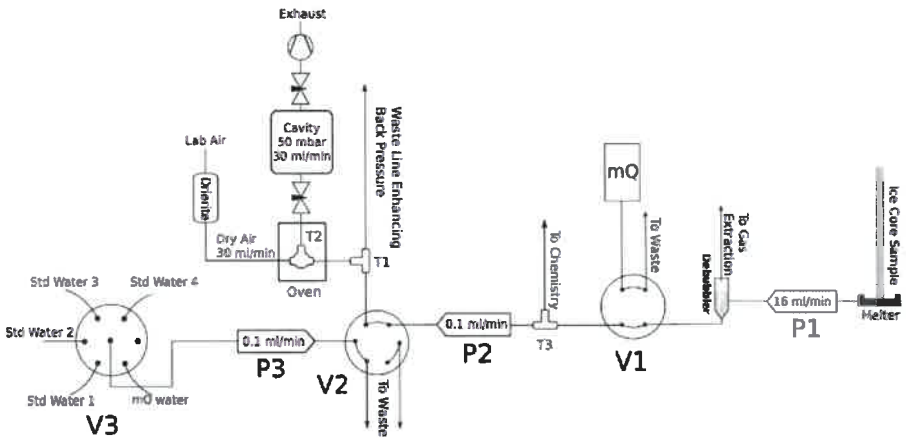

Figure 1.3: Schematic of the parts of the CFA system at PICE used for water isotope measurements. Taken from [14]

analysis are separated by a T-split T3. Pump P2 transports the water to valve V2 from which the sample is transported to an oven. In the oven, the sample is fully evaporated at 170°C and sent to the CRDS for isotopic measurements. The stainless steel tube between the oven and the CRDS is heated to around 90°C to avoid recondensation of the sample that can cause fractionation and memory effects. The background signal in the CRDS is kept low by the dry air, as in the discrete sampling setup.[12][14]

V2 is also connected to valve V3, which in turn is connected to up to four sources of standard water with known isotopic compositions and to an additional milliQ water source. At the beginning and end of the day the standards are measured with the CRDS. This procedure helps to calibrate for any instrumental drifts.[12][14]

Compared to discrete sampling, CFA is faster, as up to 12m of ice core can be measured within a day. However, CFA needs constant manual input, whereas in discrete sampling it is not necessary. In CFA, a new ice sample rod needs to be manually mounted in the freezer each time when a previous one has been melted. In addition, the timestamp of the sample change needs to be noted down and the system flushed with milliQ water. As an advantage, using CFA with CRDS provides a continuous water isotope record.

1.3 Laser Ablation

Laser ablation is the removal of material by sputtering, which is defined as beam-induced ejection of particles from surfaces. Ideally laser ablation leaves the surface of the material structurally or com-

positionally modified at mesoscopic length scales, while preserving the strength of the native material. Historically, a controlled and repeatable laser ablation, where target material phase is directly changed from solid to gas, wasn't possible since the typical electron-hole thermalization times were much shorter than the typical laser pulse duration. However with the invention of picosecond and femtosecond pulse lasers, clean laser ablation is possible, as the energy is deposited locally and doesn't have time to spread into the surrounding material.[15]

Laser ablation is a widely used technique for micromachining metals and it has been researched for various types of metals and laser parameters. It is less commonly used for dielectrics, such as fused silica [16], sapphire [17], and also ice [18]. The microscopic mechanism for ablation in dielectrics is that the laser pulse creates self-trapped excitons, which thereafter produce mechanical motion and heat in their local surroundings, through electron-phonon coupling. The created vibrations are strong enough to break bonds of the crystal structure, leading to damage of the targeted material, resulting in ablation.[15]

A useful quantity to describe the impact of the laser pulse is the fluence F, which shows the energy of the pulse deposited onto the surface of the material, per unit area. Each material has a certain fluence thershold, which describes the minimal fluence of a pulse required for any ablation to occur. The existence of such a threshold has been demonstrated by an experiment with SiO_2, where no damage was observed after 10000 shots with a pulse energy 2% below the fluence threshold.[16]

Aside from the pulse energy, the pulse repetition rate also plays an important role. For low repetition rates, each pulse is independent from the previous one, and each pulse must individually exceed the fluence threshold for ablation to occur. For higher repetition rates, the effects of each pulse are compounded and they may create multiple coexisting excitons, which lead to melting and other thermal effects. These effects have been studied theoretically [15], but have not been experimentally analyzed for ice in a systematic study.

The radius of the minimal spot size that a Gaussian laser beam can be focused in is determined by diffraction limit [19][20]

$$\omega_0 = \frac{M^2 \lambda f}{\pi \omega_f} \cdot \frac{1}{\sqrt{1 + (M^2 \lambda f / \pi \omega_f^2)^2}} \simeq \frac{M^2 \lambda f}{\pi \omega_f}, \tag{1.16}$$

where M^2 is the beam quality factor, λ is the wavelength of the laser, f is the focal length of the lens and ω_f is the beam radius before the lens. Due to the manufacturing limitations of lenses, the focal length will be at least as large as the spot size before focusing. As a consequence, the minimal achievable spot size will be comparable to the wavelength of the laser. As a result, UV-lasers are the preferred choice in laser ablation applications. However, the absorption coefficient of ice in the UV range of commercially

available high power femtosecond lasers is up to 10^4 times smaller than in the near infrared region. A lower absorption coefficient means that less energy is transferred from the laser to the ice, resulting in a lower ablation rate.

Figure 1.4 shows the absorption spectrum of ice [21], including examples of wavelengths used in some laser ablation experiments performed on ice by different groups. In general, there are not many examples in the literature of laser ablation being used on ice, and existing examples involve mostly either UV or IR wavelengths. The selection of experiments included in the figure is representative of the research conducted in this field. One work in particular, (Reinhardt, et al.) used an IR laser similarly to the one in this work, based on the same reasoning as described in the previous paragraph.

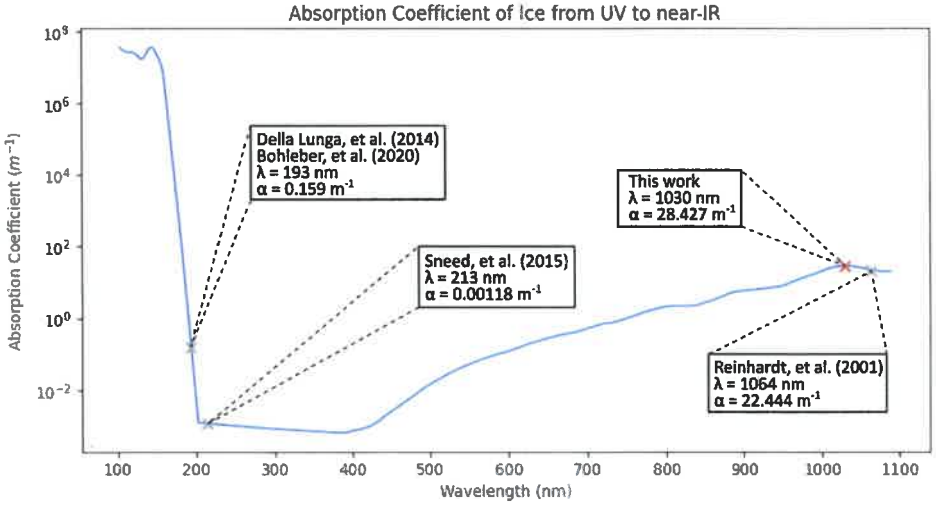

Figure 1.4: The absorption coefficient α of ice with respect to the wavelength λ (blue line) with $\times$-s marking different works done in field of laser ablation of ice cores.

Table 1.2 shows more information on the articles. All of the articles focus on analyzing chemical impurities in ice cores. The detection method used is inductively coupled plasma mass spectrometry (ICP-MS), but the ice sample size that can be accommodated differs from system to system.

	Research Branch	Detection Method	Dimensions of an Ice Sample
Bohleber, et al. [18]	chemical impurities	ICP-MS	80mm × 20mm × 15mm
Della Lunga, et al. [22]	chemical impurities	ICP-MS	50mm × 11mm × 11mm
Reinhardt, et al. [23]	chemical impurities	ICP-MS	⌀100mm × 10mm 100mm × 50mm × 10mm
Sneed, et al. [24]	chemical impurities	ICP-MS	1000mm × 30mm × 30mm
Spaulding, et al. [25]	chemical impurities	ICP-MS	1000mm × 30mm × 30mm
This work	water isotopes	CRDS	550mm × 30mm × 30mm

Table 1.2: Overview of the research branch, detection method and dimension of the ice sample used in the existing literature on laser ablation of ice cores.

CHAPTER 2

Experimental Methods

2.1 Overview of the Laser Ablation System

Motivation

Laser Ablation (LA) is a relatively new, but promising technique in ice core research next to discrete sampling and CFA. The latter two require an ice sample as a whole to be melted in order to preform measurements, whereas LA is non-destructive, requiring only a small part from the surface of the sample. The resulting crater in ice from LA is in the range of few tens to few hundreds of micrometers, with the exact size depending on the optics, measurement strategy and the coupling efficiency to the detection tool.

LA is also a faster method, as only a small part of the ice sample is measured and it is directly vaporized, instead of using the whole sample and melting the sample before vaporizing it. In addition, due to the size of the resulting craters, high resolution measurements can be made by scanning the laser along the width of the ice sample. Meaning that at depths where the annual layers of ice cores have thinned to an order of few millimeters or less, it is possible to obtain multiple data points with LA.

Developing a new, faster, non-destructive, high resolution method is especially important in light of the Beyond EPICA project. In this project, the oldest ice core in the world will be drilled in Antarctica. This ice core contains climate history of up to 1.5 million years, with annual layers decreasing down to around one hundred micrometers.

Short Description of the System

During this thesis, the laser ablation system at PICE is built from scratch. This system is made for measuring water isotopes and it will interface CRDS that is used as a detection tool. A small scale proof-of-concept experiment was conducted at the Technical University of Denmark (DTU), prior to building a system at PICE. This experiment successfully utilized a high power femtosecond laser with CRDS to detect change in water vapour when performing laser ablation on an ice sample. The description of experiment conducted at DTU can be found in the results chapter.

One of the key requirements for the system at PICE was being able to accommodate an ice sample with dimensions of 30mm × 30mm × 550mm. This is important as these dimensions correspond to one of the standard ice core sample sizes. This allows an ice core that is used for LA to be used later for other measurements (e.g. chemical impurities with CFA).

The system at PICE consists of three main parts:

1. Mechanical Translation
2. Optical Setup
3. Gas Flow

The central object for all of the three parts is a freezer, which is mounted on a frame constructed from aluminium profiles. An optical table is mounted on the same frame next to the freezer (Figure 2.1), so that they are level with each other.

The laser beam is directed from a femtosecond IR laser on top of the optical table into the freezer. The beam is then directed down onto the ice by optical components mounted on the another aluminium frame inside the freezer. Additionally, this aluminium frame holds a linear stage, which is the main component of the mechanical translation part. The aluminium frame inside the freezer ensures that the linear stage is perpendicular to the rail where the optical components are mounted.

There are three holes drilled in the freezer. The first is for the laser beam to go through, the second is for the dry gas flow and the third is for the pipe interfacing a cavity ring down spectrometer (CRDS) and for electrical wires. The latter also includes signal, power and ground wires for DTH22, which is a simple digital sensor connected to a Arduino Uno board. The DTH22 sensor is attached to the aluminium frame inside the freezer, close to the lid of the freezer. The sensor monitors temperature and humidity inside the freezer at all times.

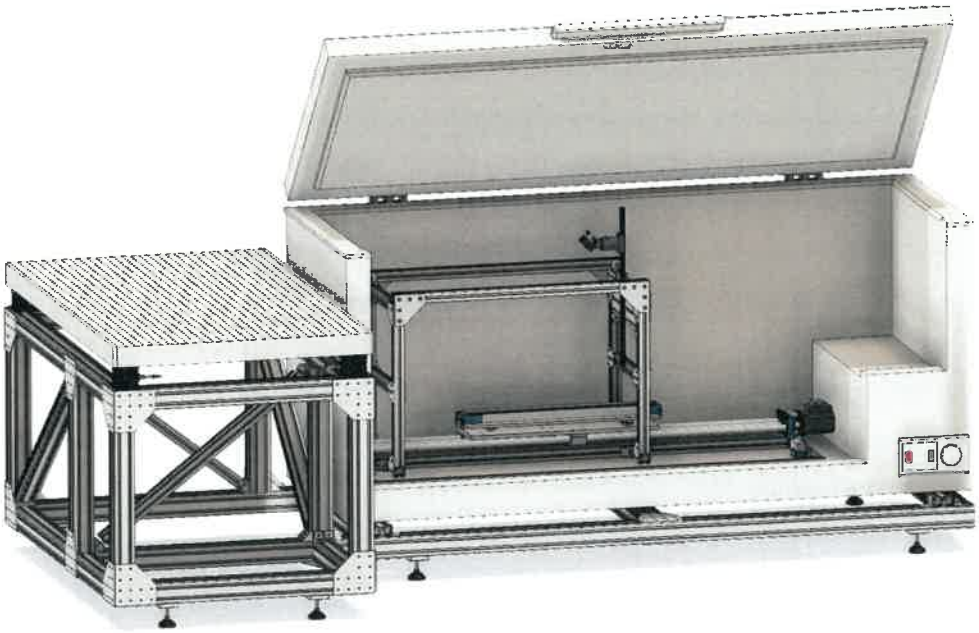

Figure 2.1: The optical table and freezer are mounted on the same aluminium frame. Inside the freezer there is another frame where linear stage and a rail for optical components are mounted.

The samples used in this work in the laser ablation experiments are made from milliQ water. They are cut from ice cylinders using a band saw in a cold room at around $-19°C$. The ice samples are then manually scraped with a microtome blade to ensure a smooth surface of the sample. For identification purposes we make markings on the ice surface in designated places. These are made with a ceramic knife in between ablation experiments.

This chapter gives an overview of all of the three parts including the associated electronic components and software written specifically for this laser ablation system.

2.2 Mechanical Translation

The purpose of the mechanical translation system is to move an ice sample underneath the laser beam with the help of a remote control. This is important, because it allows us to perform tests at different sections of the top surface of the ice sample without needing to open the freezer in order to adjust the sample. The ability to control the mechanical translation system remotely is necessary to perform experiments time efficiently. In addition, it decreases the amount of times the system is disturbed by opening the lid. The latter would result in a temperature and gas concentration change as well as condensation on the optical elements inside the freezer.

Mechanical Components

The central object of the mechanical translation part is a linear stage, which is fixed to the aluminium profile frame inside the freezer. The aluminium profile frame, that holds the linear stage and the optical components, is mounted onto wood plates with bead positioning screws. The frame can be lifted outside of the freezer if necessary and when putting it back, the same location of the frame with respect to the freezer is ensured by the bead positioning screws.

The chosen linear stage is sold by a German company called DOLD Mechatronics and its product name is *Easy-Mechatronics System 1216A nominal length 1200mm*. The nominal length of the linear stage accommodates an ice sample with the standard dimensions of 30mm × 30mm × 550mm. The linear stage has a base made of 30 × 120L I-type groove 6 aluminum profiles to which two shafts and a ball screw with linear bearings are attached with the help of metal plates.

The tray, along with the base (Figure 2.2) that attaches to the linear bearings of the linear stage, is made from plexiglass. The ice sample in the tray is held in place during an experiment with adjustable plexiglass walls. The tray allows for manual transverse repositioning of the ice sample by adjustment of the plexiglass walls. The base of the tray is mounted to the linear bearings with M6 screws. The base attaches to the tray with magnetic kinematic seats glued to both of the parts. This ensures that the location of the tray with respect to the base always stays the same. This is convenient whenever the tray needs to be removed in order to change and/or inspect the ice sample.

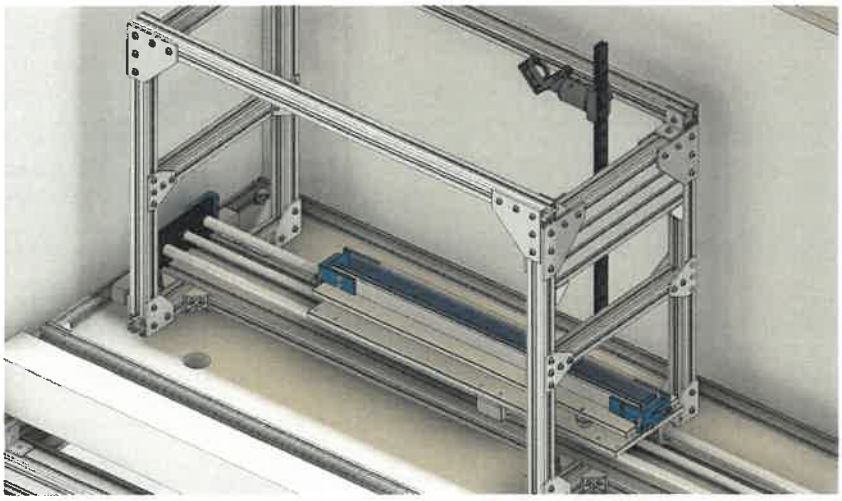

Figure 2.2: The tray holding an ice sample is attached to the linear stage. The black rail used for mounting optical components and hole in the bottom of the freezer for electrical wires can also be seen in this picture.

Electronics

The main electronic components used in this project are a stepper motor and two endstops controlled by an Arduino Uno board. The schematics of the electronics and their mutual connections are shown in Figure 2.3.

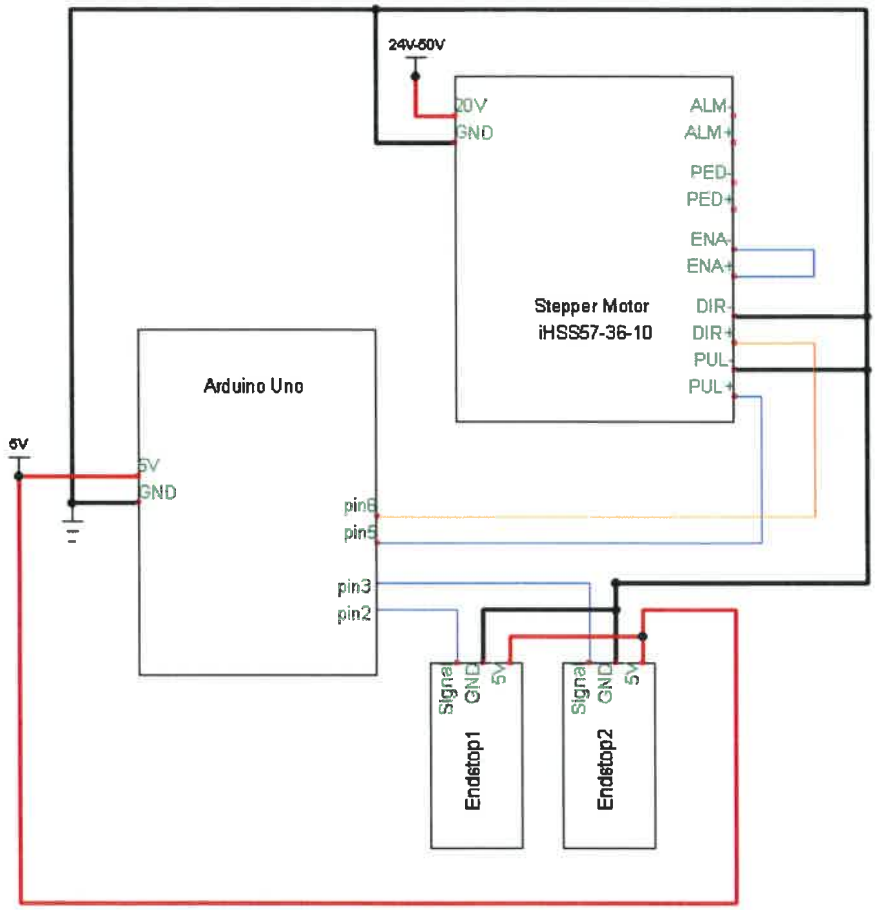

Figure 2.3: Schematics of the electronics used for the mechanical translation system.

The ball screw of the linear stage interfaces a stepper motor. The stepper motor used for this project is *iHSS57-36-10*. This is a stepper motor with an integrated driver from a Chinese company called Just Motion Control. The shaft of the motor is attached to the ball screw of the linear stage by a shaft coupling. The rotational movement of the shaft and the ball screw is translated to linear movement of the tray that holds the ice sample.

The stepper requires $24 - 50$VDC input voltage and can be controlled with 5VDC or 24VDC input signals [26]. In this project the stepper motor is controlled by the Arduino Uno board. We use two input

pins DIR and PUL connected to the common ground. Sending 5V or 0V from the Arduino Uno board to DIR pin causes the stepper motor to move clockwise or counterclockwise respectively. Sending a 5V pulse to the pin PUL causes the motor to move one step.

The number of steps per revolution is determined by a microstepping setting. This can be set by toggling the physical dial switches on the motor [26]. In our application the number of microsteps is 800. The linear distance covered by the tray on the linear stage in one revolution is determined by the pitch length of the ball screw. The pitch of the ball screw used for this project is 4mm.

The stepper motor was tested in the cold room at $-19°C$ at PICE. The motor preforms without any problems at low speeds (e.g. 0.5mm/s) and at high speeds (e.g. 20mm/s). For this application we mostly use speed 5mm/s when moving the ice between measurements or when calibrating the linear stage.

Two mechanical endstops are used for both calibration of the position of the tray and for safety purposes. They are placed to the both ends of the linear stage and have three pins 5V, GND and signal. The endstops are normally closed. This means that when the mechanical switch is free the circuit is closed and 5V is read from the signal pin by the Arduino Uno board. If the tray comes in contact with either of the two endstops, the mechanical switch is pushed down and 0V is read from the signal pin. This change in signal is detected in the Arduino Uno board.

2.3 Optical Setup

The purpose of the optical setup is to guide the beam from the high power femtosecond IR laser, which is mounted on the optical table, onto the ice sample, which is placed in tray located in the bottom of the freezer.

The optical setup comprises of a high power femtosecond infrared laser, a red guiding laser, a focusing lens, and mirrors for directing the laser beam from the two lasers onto the ice sample. In addition, the safety components are counted as a part of the optical system. The model name of the IR laser is *ORIGAMI XP* and it is manufactured by the Danish company called NKT Photonics. The red guiding laser and most of the other optical components are produced by a USA company called Thorlabs.

The IR laser used for ablation has a wavelength of 1030nm and a pulse duration of 400fs. The laser beam propagates with a TEM_{00} profile. The beam quality factor, that describes the deviation from a Gaussian beam, is $M^2 = 1.2$. The average maximum power of the IR laser is 4W and the maximum energy per pulse is 40uJ. The repetition rate of the laser goes up to 1MHz. In this project we use

repetition rates 50kHz and 100kHz, since this allows us to access the pulse energy of 40uJ. A repetition rate of 100kHz with pulse energy 40uJ already uses the maximum available power $100\text{kHz} \cdot 40\text{uJ} = 4\text{W}$. Therefore, higher repetition rates can only be used for lower pulse energies.

The optical components are mounted both onto the optical table and onto the rail located inside the freezer. This is necessary to guide the laser beam onto the ice sample. The components on the optical table are shown on Figure 2.4. The table is surrounded with black anodized aluminium protective screens for protection against scattered laser light. The IR laser and the guiding laser are mounted on the opposite sides of the table. The beam diameter of the guiding laser is decreased with a plano-convex lens L1 ($f = 75\text{mm}$) and a bi-concave lens L2 ($f = -25\text{mm}$). The beams from the two lasers are then aligned by bringing them together with the mirrors M1-M4 at the dichroic mirror DM.

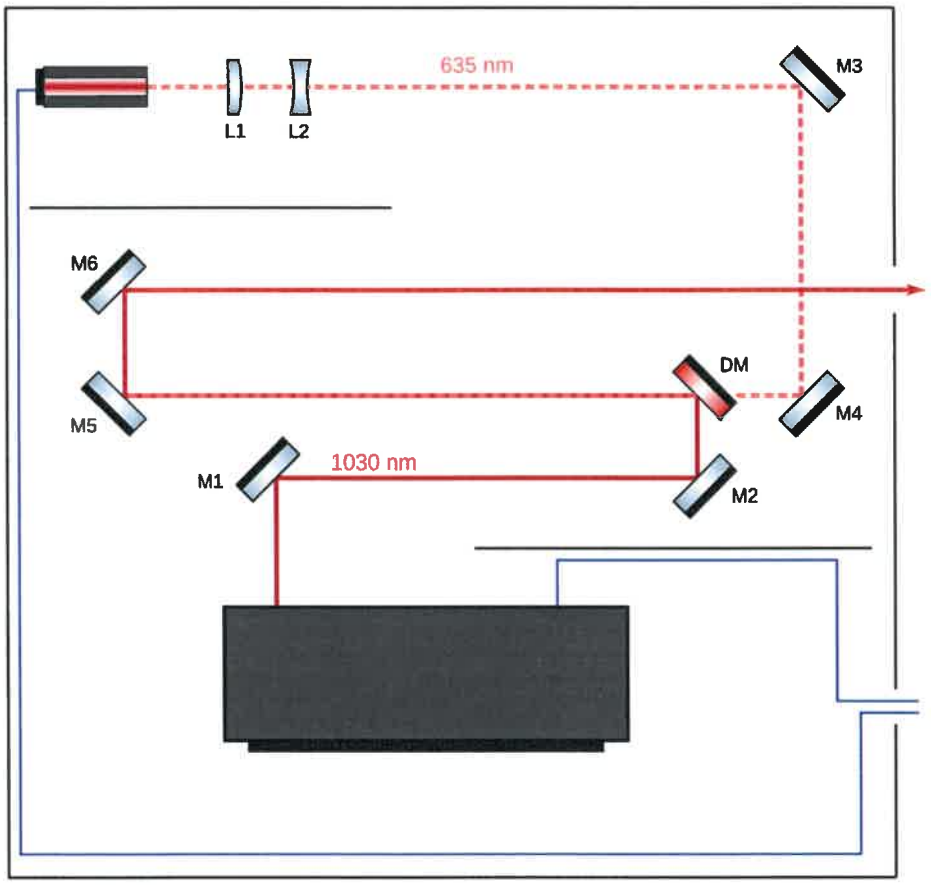

Figure 2.4: The optical setup on top of the optical table. Black lines are anodized aluminium screens. Blue lines are power (IR, guiding) and signal (IR) wires.

The cutoff wavelength λ_{cutoff} of the dichroic mirror is 650nm. This means that for a laser with wavelength

λ, most of the light is transmitted when $\lambda < \lambda_{\text{cutoff}}$ and most of the light is reflected when $\lambda > \lambda_{\text{cutoff}}$. The wavelength of the guiding laser is 635nm which corresponds $T = 97.0\%$ transmission through the dichroic mirror. The wavelength of the IR laser is 1043nm corresponding to $R = 98.1\%$ reflection from the dichroic mirror.[27]

After the two beams are aligned, the mirrors M5 and M6 are used to direct the beams first through a hole in the protective screen and then through a hole in the freezer. The beam coming from M6 finally arrives at mirror M7 mounted in the freezer (Figure 2.5). M7 is placed at a 45° angle, reflecting the beam down to the beam expander BE. The beam coming from the beam expander gets then focused by the plano-convex lens L3 ($f = 50$mm) onto the ice sample. The walls and the lid of the freezer are covered with black anodized aluminium foil to protect against any scattering of the light from the optics or from the ice sample.

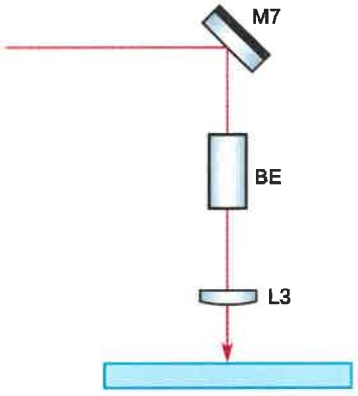

Figure 2.5: The optical setup in the freezer.

The radius of the spot size of the laser beam after the focusing lens L3 can be calculated from Equation 1.16 presented in the Laser Ablation chapter. The spot diameter achieved with the focusing lens is then

$$d = \frac{4\lambda M^2 f}{\pi d_f}, \tag{2.1}$$

where λ is the wavelength of the laser, M^2 describes the deviation of the beam from Gaussian, f is the focal length of the lens. The beam diameter before the lens is $d_f = m \cdot d_{\text{BE}}$, where m is the magnification of the beam expander and d_{BE} is beam diameter before the beam expander.[19][20]

The smallest spot of the beam is called the beam waist. The depth of focus achieved with the focusing lens is described by the Rayleigh length z_R. The Rayleigh length is described as the distance from the beam waist to the point where the beam diameter has increased by multiple of $\sqrt{2}$. The equation for

Rayleigh length is

$$z_R = \frac{\pi d^2}{4\lambda M^2}, \tag{2.2}$$

where d is the diameter of the beam at the beam waist. [20]

The depth of focus covers the Rayleigh length on both sides of the beam waist and can therefore be written as [20]

$$\text{DOF} = 2z_R = \frac{\pi}{2\lambda M^2} d^2 = \frac{\pi M^2}{2\lambda} \left(\frac{4\lambda f}{\pi d_f}\right)^2 = \frac{8\lambda M^2}{\pi} \left(\frac{f}{d_f}\right)^2. \tag{2.3}$$

The beam expander considered for this application has a magnification range of 2X, 3X,.., 8X. The focused beam diameter and DOF are shown on Figure 2.6 for different magnifications and lenses with three different focal lengths. The data on this figure gives an approximate idea of the spot size and DOF. The focusing lens chosen for this application has a focal length f = 50mm. The beam expander was

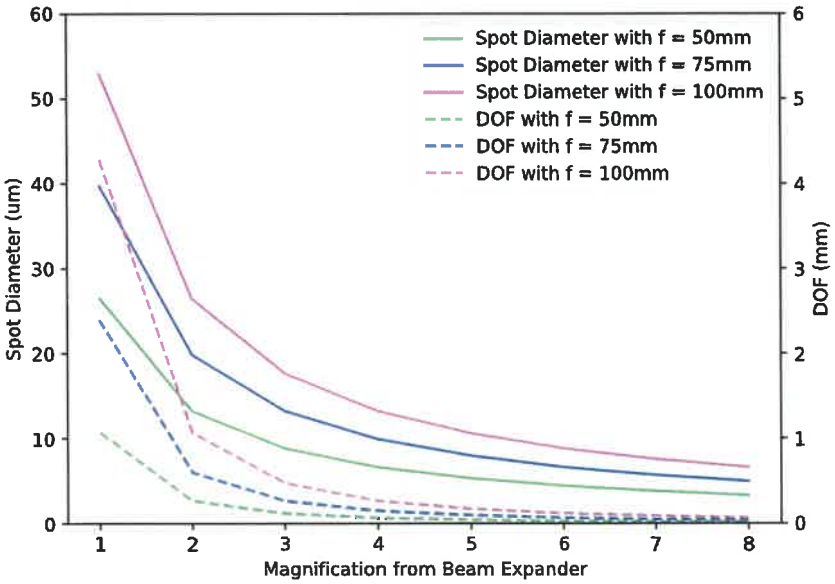

Figure 2.6: Focused spot diameter and depth of focus with respect to the magnification of the beam expander for different focal lengths of the focusing lens.

not used for the specific results presented in this thesis. This is due to condensation problems explained further in the section describing the gas flow system. In addition, using no beam expander makes the focusing simpler as the depth of focus is larger. However, for future experiments, the beam expander would be a useful component that improves the performance of the laser ablation system.

2.4 Software

The purpose of the software written for the laser ablation system at PICE is to control the femtosecond IR laser and the linear stage, as well as to provide feedback to the user. The code is available at `https://github.com/kerttumariap/Laser_Ablation.git`. The software consists of six different files.

- **linear_stage.json** stores information about the specific stepper motor, linear stage and the ball screw used for the project.
- **linear_stage.ino** is low level code run on the Arduino Uno board that sends signals to the stepper motor and receives signals from the two endstops. In addition, it receives commands from the user and sends feedback.
- **linear_stage.py** is a class called *LinearStage* that gets information from *linear_stage.json* when initialized. It is a high level Python code that establishes a serial connection and exchanges information with *linear_stage.ino*. It has methods for serial communication and unit conversions.
- **laser.py** is a class called *Laser*. It is a high level Python code that establishes a serial connection and exchanges information with the IR laser using RS-232.
- **LA_main_v2.py** is Python code, which has two classes: *App*, the graphical user interface (GUI) built with a library called PyQt5, and *WorkerThread*, for the working thread. The first creates the GUI with it's visuals, it shows information about the linear stage and the laser, as well as receives inputs from the user. The second runs the working thread, it creates an instance of the classes *LinearStage* and *Laser*. The working thread sends and receives information about the stepper motor and the IR laser using methods of the classes *LinearStage* and *Laser* respectively. Information received is logged into a tab delimited file.
- **general_functions.py** stores functions used by the user interface class *App*.

The GUI (Figure 2.7) consists of two main parts: Linear Stage Control and Laser Control. The different parts of Linear Stage Control are described in the following list.

- **Direction** has two values 1 and -1. The first corresponds to the tray moving to the right and the second to the left.
- **Speed** can be specified in four different units mm/s, rev/s, steps/s or as a time delay between each step in µs.
- **Distance** can be specified in three different units: mm, rev and steps. Choosing a value for the distance and clicking the button "Move" causes the tray to travel that distance with current speed to the currently specified direction.

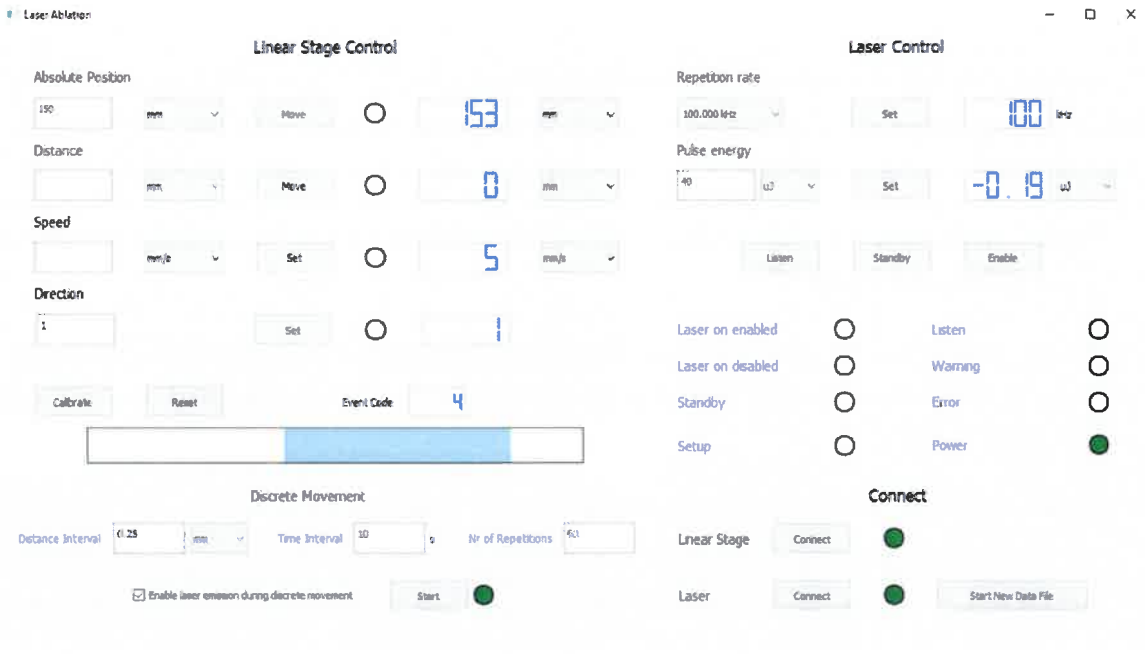

Figure 2.7: The graphical user interface of the laser ablation system.

- **Absolute position** can be specified in the same units as the distance. The sign of the input determines the direction of the movement. The position at startup corresponds to 0mm. It is redefined at the center of the linear stage after the calibration has been run.
- **Calibrate** sets the absolute position 0mm in the middle of the linear stage and positions the center of the tray there. This is done by driving the tray to the one end of the linear stage which is registered by the mechanical endstop. Then the steps are counted while driving the tray to the other endstop. Next the tray is placed to the half of the measured distance and absolute position is set to 0mm. After calibrating the stage a figure that shows the placement of the tray with respect to the linear stage becomes available (Figure 2.8).

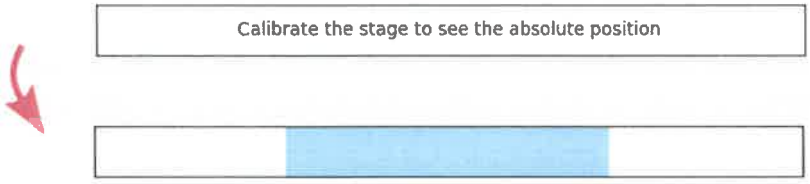

Figure 2.8: The absolute position of the tray with respect to the linear stage can be seen once the stage has been calibrated.

- **Reset** stops the movement of the tray and terminates the ongoing movement of the tray, e.g. calibration.
- **Discrete Movement** moves the tray in discrete intervals, which can be specified in mm, rev or in steps. The time interval in between movements during which the tray is idle, is specified in seconds. Number of repetitions determines the number of distance intervals covered. The IR laser is enabled during idle phase of the discrete movement, if the box 'Enable laser emission during discrete movement' is checked. The pulse energy and repetition rate used for the laser are the ones specified the latest by the user.

The repetition rate and the pulse energy can be set using Laser Control. The repetition rate is in kHz and it is possible to choose from the ten repetition rates specified by the manufacturer of the laser. The pulse energy can be set both in µJ and nJ. The status of the laser is displayed on the LED array (table 2.1). LED that is ON shows colour green and LED that is OFF shows colour gray.

LED Name	Description
Laser on enabled	Laser is ON. If the shutter is open, the laser emits class 4 radiation
Laser on disabled	Laser is ON, but emission is reduced to low values. The emissions are still rated class 4.
Standby	The laser has thermalized (warmed up), but the high power pump is not enabled. The residual leakage radiation is rated class 4.
Setup	The laser is booting up. The laser does not emit radiation.
Listen	Only the microprocessor is running. The laser does not warm up or emit radiation.
Error	There is an error code active.
Warning	The laser has reached a critical temperature.
Power	DC power is connected to the laser.

Table 2.1: The different LED indicators in the GUI and their descriptions. Descriptions are specified by the manufacturer.

2.5 Gas Flow System

The gas flow system consists of a CRDS (working principle described in 1.2), a dry air unit, and also the freezer itself. The CRDS used in this work is the L2130-i isotopic water analyzer, manufactured by the USA company Picarro. The dry air unit is an AD70L, produced by the Scottish company Peak Scientific. The dry air unit seals the freezer from the lab environment by overpressure.

The dry air unit is connected to the freezer with a 6mm plastic tube. The interface between the dry air unit and the freezer is airtight. The first few meters of plastic tube in the freezer are coiled up. This helps the dry air get colder as it is initially at room temperature. The dry air tube is then placed evenly along one side of the freezer.

Near the mirror that directs the laser beam down to the ice sample, the dry air tube is split. The dry air is directed onto the mirror from both sides of the mirror. This is necessary to avoid condensation problems from occurring whenever the lid of the freezer is opened. Condensation is also one of the reasons the beam expander was removed from the setup. The beam expander has two surfaces that need to be flushed with dry air. This is necessary to avoid scattering of the IR laser beam from the beam expander. The condensation problem can be solved by reconfiguring the distribution of dry air inside the freezer.

The dry air unit supplies a dry air flow of 70l/min. At this flow rate the freezer is flushed with dry air in around 8min. A flow controller is attached to the plastic tube after the outlet of the dry air unit. The flow controller has eight settings (Figure 2.9), which allow to reduce the dry air flow when necessary.

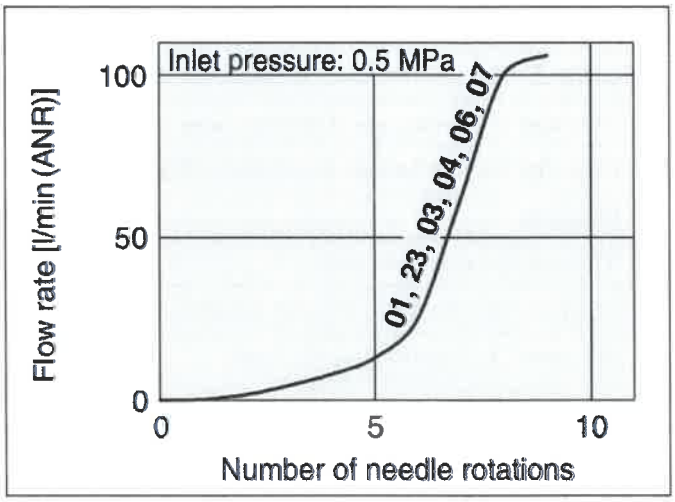

Figure 2.9: The plot shows how the flow rate is reduced with respect to the different flow control settings. The numbers on the line show the diameter (in this application 6mm). Taken from [28].

A 1/16 inch stainless steel tube interfaces the CDRS. This tube transports the water vapour from the ablated sample to the CRDS. It goes through the hole in the bottom of the freezer. This hole is stuffed with paper to avoid leakage of dry air. The third hole in the freezer is open as the laser beams pass through it. However the size of the hole is reduced with a 3D printed insert that can be positioned

correspondingly to the alignment of the laser beams.

CHAPTER 3

Results and Discussion

3.1 Proof of Concept

The first experiment performed before building a full-scale system is a proof of concept (POC) experiment, conducted at DTU. The aim of this experiment is to test laser ablation on ice on a small scale. Doing this will allow us to improve the design and implementation of a full-scale system. Additionally, we want to observe the behaviour of the IR laser used for the experiments, as most of the similar works use UV lasers instead. This test will help us to decide what optical system would be most efficient for our purposes.

The POC experiment uses an ORIGAMI 10XPS femtosecond infrared laser. The cavity ring down spectrometer used in this experiment is an L2130-i isotopic water analyzer. In addition, the setup has multiple other components, which we designed or chose specifically for this experiment.

First, we describe the cryocell (Figure 3.1), which is an aluminium container meant for holding the ice sample. The material is chosen for its good heat conductivity, so it can complement the cooling system. The shape of the cryocell is rectangular and it has inner dimensions of 20.4mm × 30mm × 120.4mm and outer dimensions of 39.5mm × 39.5mm × 139.5mm. This size is convenient due to the following reasons. Firstly, it can fit into the existing laser setup at DTU. Secondly, ice samples of this size are smaller and can be easily transported. Thirdly, it takes less than a day to print a set of spacers that can be used to adjust the position of the ice sample or to fill up the dead volume in this cryocell.

Figure 3.1: Two different views of the cryocell.

The cryocell also has a separate lid (Figure 3.2), which is 3D printed from PLA filament. The lid is made out of a different material compared to the cryocell, because it makes trying out different designs for the lid more convenient as we have an access to a 3D printer. There is ⌀2mm hole inside the lid that acts as an open split as well as an entrance for the laser beam.

Figure 3.2: Two different views of the lid.

Second, we describe the inlet system which transports the vaporized sample to the CRDS (Figure 3.3). There are two NPT 1/8 inch pipe threads cut to two opposite sides of the cryocell. One makes a connection to the carrier gas source using 1/8 inch brass tubing. The other makes a connection to short 1/4 inch stainless steel tube, inside of which there is freely placed 1/16 inch stainless steel tubing. The latter introduces water vapor from an ice sample to the CRDS. The interface between the two stainless steel tubes also acts as the second open split of the system, the first one being the hole in the lid. The cryocell is sealed from the environment with over pressure making both open splits outlets of excess air.

Third, we have cooling systems for the carrier gas and the cryocell. Both need cooling to assure that an ice sample does not melt due to the temperature of the environment. The carrier gas is cooled passively, as the tubing passes through a container of liquid nitrogen. An alternative, dry air, is not used as the

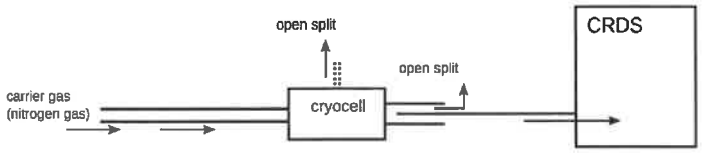

Figure 3.3: Schematic of the inlet system which transports the vaporized sample into the CRDS. Double lines denote 1/8 inch brass tubing and 1/4 inch stainless steel tube. Single line denotes 1/16 inch stainless steel tubing.

condensation temperature of oxygen is higher than the temperature of liquid nitrogen and increased oxygen levels can be a fire hazard.

The cryocell is cooled by three Peltier elements attached next to each other to the bottom of the cryocell. The elements operate by the thermoelectric phenomenon called the Peltier effect. When direct current is applied to the element, heat is transferred from one side of the Peltier device to another. The efficiency of the device depends on the temperature difference between the hot and cold side. In our system the excess heat from the hot side is removed by pumping cold water underneath it.

The laser pulses are sent through the the hole in the lid of the cryocell into the ice sample. Concurrently the water vapor concentration inside the cryocell is measured using the CRDS. We are interested in seeing a change in the background water vapour level subsequent to a laser pulse, as this means that the water vapour from the ablated ice reaches the CRDS. The pulse energy and repetition rate of the laser used are 50µJ and 100kHz respectively. The spot size of the laser is around 1mm. The laser beam itself is unfocused as the laser setup does not allow to correct that. The pressure of the carrier gas is 0.15bar throughout the experiment.

For this experiment the lid of the cryocell was chosen such that the ablation point, connection to the CRDS and the two outlets are brought to close proximity to optimize the strength of the signal. However we can still expect some of the signal to be lost as the cryocell works on overpressure. The ice sample used for the experiments has dimensions of around 15mm $\times$ 80mm $\times$ 15mm and is placed near the side of the cryocell that is connected to the CRDS. The ice fills around 24% of the cryocell and the rest of the volume is loosely filled with 3D printed spacers.

The ablation times used for this experiment are 20s, 40s and 60s. The water vapour level resulting from different ablation times are plotted on Figure 3.4. There is a clear change in water vapour level after the start of each of the three tests. This is a clear demonstration that an IR laser can indeed be used to ablate ice, and the increase in water vapour is detectable with a CRDS. This proof of concept

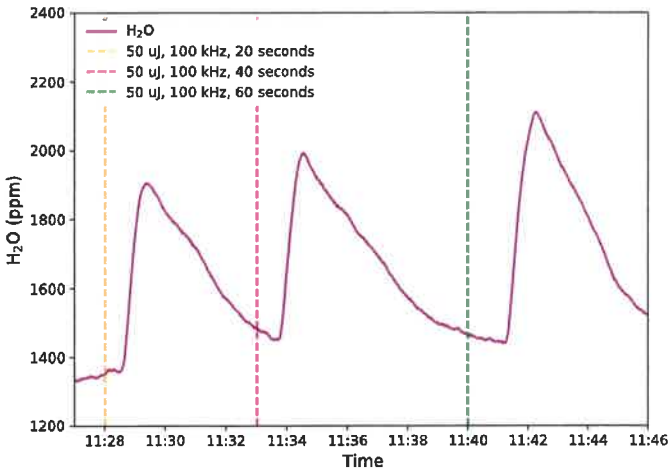

Figure 3.4: The measured change in water vapour level corresponding to three different ablation times. The three vertical lines mark the approximate start of the ablation.

enabled us to move forward with designing the full scale system.

3.2 Crater Matrix

The purpose of the crater matrix experiment was to perform a series of tests with different laser ablation parameters. In this experiment, the pulse energy and the ablation time were varied, while the repetition rate was kept constant at 50kHz. The experiment was performed using the discrete movement functionality in the software (described in 2.4) developed for this thesis. The time interval specified in the user interface is the ablation time. During the ablation time the linear stage is idle and the IR laser is enabled.

The pulse energies used in this experiment are 20uJ, 25uJ, 30uJ, 35uJ and 40uJ. The chosen ablation times are 10s, 15s, 20s, 30s and 45s. Seven craters are made for each possible pair and the distance between the centers of the consecutive craters of the same test is 1mm. The experiment is performed in five parts, as all craters are done with one pulse energy setting at the time. The steps in each of the parts are the same:

1. Scrape the chosen ice sample with a microtome blade to smooth any irregularities on the surface.
2. Fix the ice in the tray and bring the tray from the cold room into the laser ablation lab.
3. Attach the tray to the linear stage and focus the guiding laser beam onto the ice sample.
4. Close the lid of the freezer and change the dry air flow setting to 8 for 1-2 minutes. This helps to get rid of the condensation on the optics.

5. Change the air flow setting back to 4.

6. Start the ablation experiment remotely from the next room for safety purposes.

7. Bring the ice sample back to the cold room once the experiment is done for the chosen pulse energy.

8. Use a microscope to inspect and take photos of the ice sample.

The best crater out of seven is chosen after inspecting the craters for each test. These craters are presented in the crater matrix (Figure 3.5). The diameter of each crater is measured using the edge of the crater. Not all craters are perfectly round, so there remains an inherent uncertainty of the measured diameter. The crater matrix with diameter lines is in Appendix A.

The smallest crater on the crater matrix has a diameter of 83µm for pulse energy 20µJ and ablation time 10s. This is consistent with the spot diameter calculations shown in Experimental Methods chapter in Figure 2.6. The spot diameter of the focused beam is 26µm with no beam expander and lens with focal length of $f = 50$mm. This spot diameter sets a lower limit to ice crater dimension. Therefore the size of the ablated craters are expected.

On the crater matrix a trend in size of the craters can be seen. The size generally increases with the pulse energy and with the ablation time. The variability between the craters with similar parameters comes from the amount of melting that occurs at the time of the ablation. The melted ice can be also seen from the figure, when it forms a circle around the crater and/or changes the shape of the crater. Such melting can be caused by poor focusing, which in turn may originate from the fact that focusing is done manually. The melting can also occur due to uneven surface of the sample which would cause the focus quality to deviate with respect to the beam location on the the sample.

The parameters that resulted in the best craters in this experiment are listed in Table 3.1. These craters have the most circular shape and show the least signs of melting. The fact that some craters look clean and others do not, means that this laser ablation setup can be used for performing laser ablation on ice, but that it can also be optimized.

3.3 Measuring Water Vapour from Craters

The purpose of this experiment was to test whether any water vapour from the craters can be detected with our current setup. The detection tool used for measuring change in the water vapour is CRDS. The tube interfacing the CRDS is placed near the ablation point. The dry air unit is used to maintain a low water vapour level in the freezer. The flow rate setting for the dry air is 5.

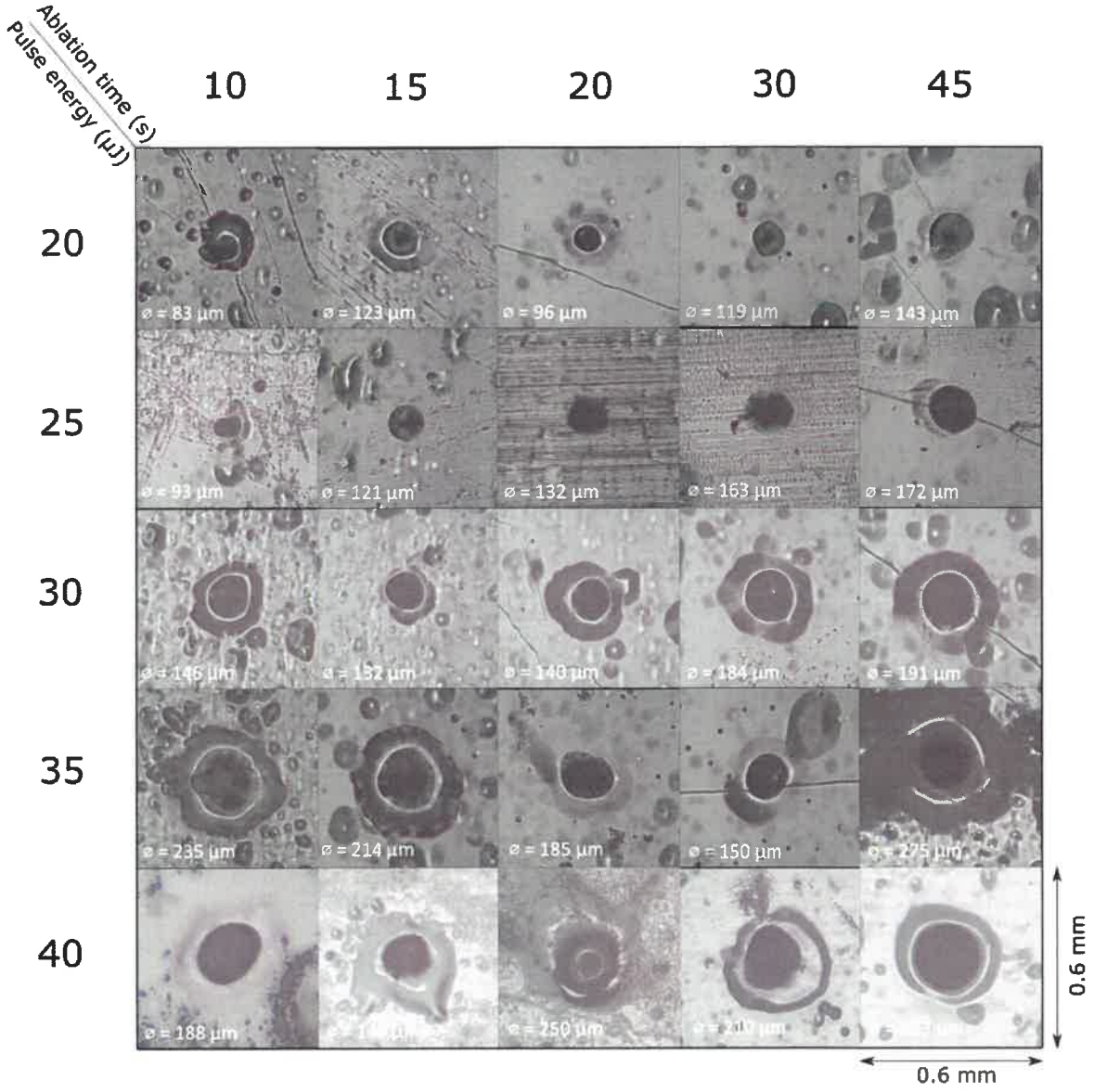

Figure 3.5: The crater matrix shows craters corresponding to different pulse energies (vertical) and ablation times (horizontal). The repetition rate of the laser is constant at 50kHz.

During this experiment two tests were performed. One with 19 and one with 30 craters. The craters were made within close vicinity using the discrete sampling setting in the software. The distance between the centers of the consecutive craters was 1mm. The ablation time for each crater was 15s. During this time, the laser was enabled and the linear stage was idle.

The pulse energy and the repetition rate used in this experiment are 40µJ and 50kHz respectively.

Pulse energy (µJ)	Ablation time (s)	Crater diameter (µm)
20	30	119
25	15	121
25	20	132
25	30	163

Table 3.1: The best craters from the crater matrix test with corresponding pulse energy and ablation time, as well as the diameter of the resulting crater.

Similarly to the crater matrix experiment, no beam expander is used in the optical setup and the focal length of the focusing lens is $f = 50$mm. The resulting water vapour from the laser ablation, as well as the ablation intervals for both tests, are shown on Figure 3.6.

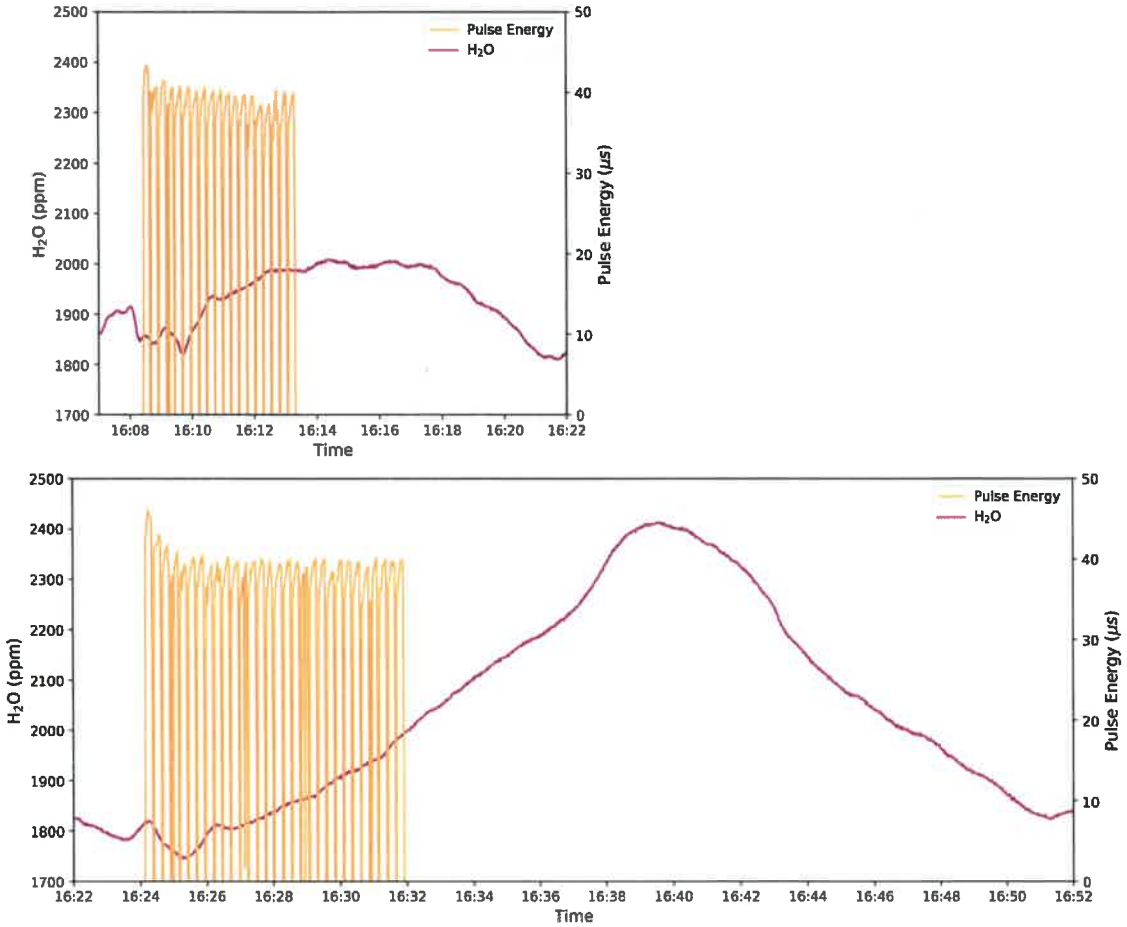

Figure 3.6: The change in measured water vapour corresponding to 19 (up) and 30 (down) ablated craters. The plots are aligned with respect to the first ablation interval.

A clear change in the water vapour level is detected as a result of laser ablation. This means that the full scale laser ablation system works. As expected, this change is greater for a larger number of ablated craters. It can be seen from the figure that the response time of the measured water vapour is delayed with respect to the laser pulses. In addition, the contribution to the water vapour level from the individual craters cannot be distinguished. The response time, resolution, and background to signal ratio could be improved by building an enclosing around the ablation spot. Connecting the tube interfacing the CRDS to the enclosing would help to catch more of the water vapour. Additionally, connecting one of the dry air lines to the enclosing would help to lower the background water vapour level measured by the CRDS.

CHAPTER 4

Conclusion and Outlook

This work describes an alternative high-resolution method for measuring water isotopes in ice cores. Using laser ablation in ice core research is relatively new and it has mostly been applied for measuring chemical impurities in ice cores. During this thesis a proof of concept experiment in small scale was conducted at Technical University of Denmark (DTU). The results from this experiment show that it is possible to vaporize ice with a high power femtosecond infrared laser (1030nm), as well as detect the water vapour with a cavity ring down spectrometer.

A full scale laser ablation system was developed from scratch at University of Copenhagen (KU), after a successful proof of concept experiment at DTU. This laser ablation system uses the same type of infared laser and cavity ring down spectrometer. The laser ablation system at KU can fit an ice sample with the standard size of 30mm $\times$ 30mm $\times$ 550mm. The ice can be moved underneath the laser beam using a remote control. The software developed for this system allows to control both the laser and the translation mechanism.

The full scale laser ablation system can be successfully used to make craters in ice. The quality of the craters can be improved by optimizing the optical setup part that focuses the laser beam on the ice. The water vapour from the ablated craters can be measured with a cavity ring down spectrometer. The background to signal ratio of the measured water vapour can be optimized by building an enclosing around the ablation spot.

Appendix A

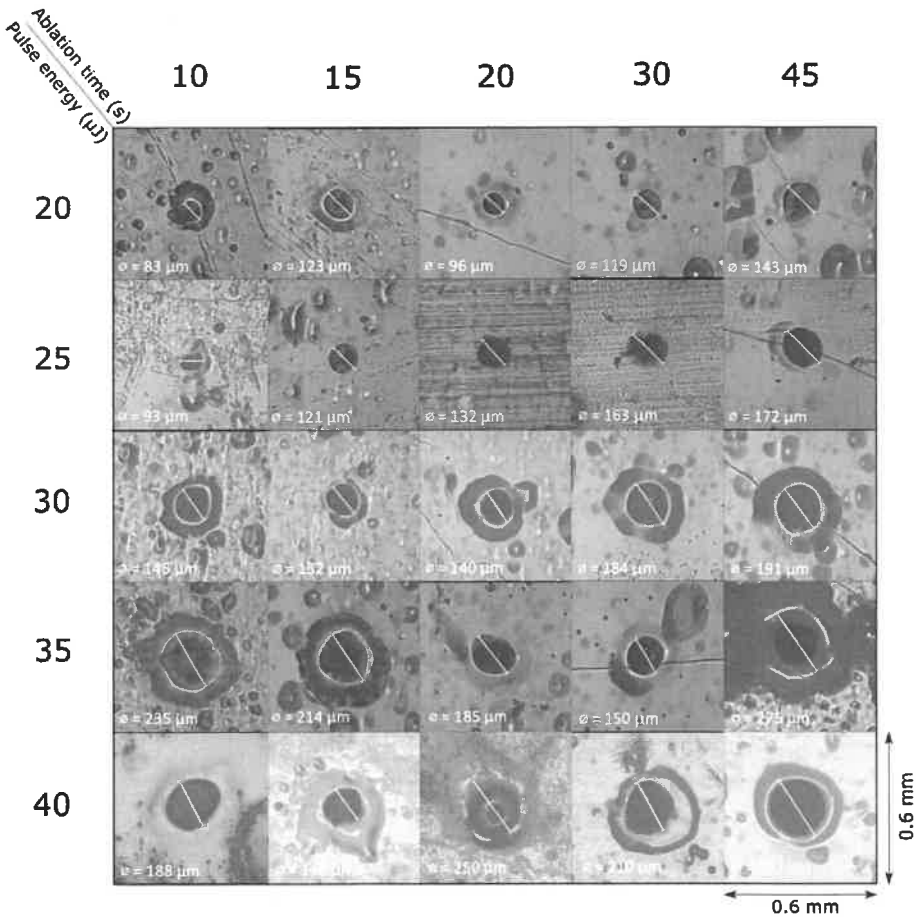

Figure 4.1: The crater matrix shows craters corresponding to different pulse energies (vertical) and ablation times (horizontal). The repetition rate of the laser is constant at 50kHz.

Bibliography

[1] David R Lide, *CRC handbook of chemistry and physics*, vol. 85. CRC press, 2004.

[2] WG Mook and Kazimierz Rozanski, "Environmental isotopes in the hydrological cycle," *Principles and Applications, Volumes I, IV and V*, 2000.

[3] Kurt M Cuffey and William Stanley Bryce Paterson, *The physics of glaciers*. Academic Press, 2010.

[4] Kurt M. Cuffey and Edward J. Brook, "18 - ice sheets and the ice-core record of climate change," in *Earth System Science* (Michael C. Jacobson, Robert J. Charlson, Henning Rodhe, and Gordon H. Orians, eds.), vol. 72 of *International Geophysics*, pp. 459–497, Academic Press, 2000.

[5] SJ Johnsen, W Dansgaard, and JWC White, "The origin of arctic precipitation under present and glacial conditions," *Tellus B: Chemical and Physical Meteorology*, vol. 41, no. 4, pp. 452–468, 1989.

[6] Sigfus J Johnsen, et al., "Oxygen isotope and palaeotemperature records from six greenland ice-core stations: Camp century, dye-3, grip, gisp2, renland and northgrip," *Journal of Quaternary Science: Published for the Quaternary Research Association*, vol. 16, no. 4, pp. 299–307, 2001.

[7] Françoise Vimeux, Kurt M Cuffey, and Jean Jouzel, "New insights into southern hemisphere temperature changes from vostok ice cores using deuterium excess correction," *Earth and Planetary Science Letters*, vol. 203, no. 3-4, pp. 829–843, 2002.

[8] Zachary Sharp, "Principles of stable isotope geochemistry," 2017.

[9] Samuel Epstein and Toshiko Mayeda, "Variation of o18 content of waters from natural sources," *Geochimica et cosmochimica acta*, vol. 4, no. 5, pp. 213–224, 1953.

[10] BH Vaughn, et al., "An automated system for hydrogen isotope analysis of water," *Chemical Geology*, vol. 152, no. 3-4, pp. 309–319, 1998.

[11] ER2008 Crosson, "A cavity ring-down analyzer for measuring atmospheric levels of methane, carbon dioxide, and water vapor," *Applied Physics B*, vol. 92, no. 3, pp. 403–408, 2008.

[12] Vasileios Gkinis, Trevor J Popp, Sigfus J Johnsen, and Thomas Blunier, "A continuous stream flash evaporator for the calibration of an ir cavity ring-down spectrometer for the isotopic analysis of water," *Isotopes in environmental and health studies*, vol. 46, no. 4, pp. 463–475, 2010.

[13] Willi A Brand, Heike Geilmann, Eric R Crosson, and Chris W Rella, "Cavity ring-down spectroscopy versus high-temperature conversion isotope ratio mass spectrometry; a case study on delta (2) h and delta (18) o of pure water samples and alcohol/water mixtures," *Rapid communications in mass spectrometry: RCM*, vol. 23, no. 12, pp. 1879–1884, 2009.

[14] V Gkinis, et al., "Water isotopic ratios from a continuously melted ice core sample," *Atmospheric Measurement Techniques*, vol. 4, no. 11, pp. 2531–2542, 2011.

[15] John C Miller and Richard F Haglund, *Laser ablation and desorption*, vol. 30. Elsevier, 1998.

[16] BC Stuart, et al., "Nanosecond-to-femtosecond laser-induced breakdown in dielectrics," *Physical review B*, vol. 53, no. 4, p. 1749, 1996.

[17] Mehrnaz N Christensen, Jeppe Byskov-Nielsen, Bjarke H Christensen, and Peter Balling, "Single-shot ablation of sapphire by ultrashort laser pulses," *Applied Physics A*, vol. 101, no. 2, pp. 279–282, 2010.

[18] Pascal Bohleber, Marco Roman, Martin Šala, and Carlo Barbante, "Imaging the impurity distribution in glacier ice cores with la-icp-ms," *Journal of Analytical Atomic Spectrometry*, vol. 35, no. 10, pp. 2204–2212, 2020.

[19] Roberto Osellame, Giulio Cerullo, and Roberta Ramponi, *Femtosecond laser micromachining: photonic and microfluidic devices in transparent materials*, vol. 123. Springer Science & Business Media, 2012.

[20] PW Milonni and JH Eberly, *Laser Physics*. John Wiley & Sons, 2010.

[21] Stephen G Warren and Richard E Brandt, "Optical constants of ice from the ultraviolet to the microwave: A revised compilation," *Journal of Geophysical Research: Atmospheres*, vol. 113, no. D14, 2008.

[22] Damiano Della Lunga, Wolfgang Müller, Sune Olander Rasmussen, and Anders Svensson, "Location of cation impurities in ngrip deep ice revealed by cryo-cell uv-laser-ablation icpms," *Journal of Glaciology*, vol. 60, no. 223, pp. 970–988, 2014.